Journal of
Synchrotron Radiation

ISSN 0909-0495

Received 18 January 2013
Accepted 30 July 2013

Energy calibration issues in nuclear resonant vibrational spectroscopy: observing small spectral shifts and making fast calibrations

Hongxin Wang,[a,b]* Yoshitaka Yoda,[c] Weibing Dong[a,d] and Songping D. Huang[e]

[a]Department of Chemistry, University of California, 1 Shields Avenue, Davis, CA 95616, USA, [b]Lawrence Berkeley National Laboratory, 1 Cyclotron Road, Berkeley, CA 94720, USA, [c]JASRI, SPring-8, 1-1-1 Kouto, Sayo-cho, Sayo-gun, Hyogo 679-5198, Japan, [d]Liaoning Provincial Key Laboratory of Biotechnology and Drug Discovery, Liaoning Normal University, Dalian 116081, People's Republic of China, and [e]Department of Chemistry and Biochemistry, Kent State University, Kent, OH 44242, USA. E-mail: hxwang2@lbl.gov

The conventional energy calibration for nuclear resonant vibrational spectroscopy (NRVS) is usually long. Meanwhile, taking NRVS samples out of the cryostat increases the chance of sample damage, which makes it impossible to carry out an energy calibration during one NRVS measurement. In this study, by manipulating the 14.4 keV beam through the main measurement chamber without moving out the NRVS sample, two alternative calibration procedures have been proposed and established: (i) an *in situ* calibration procedure, which measures the main NRVS sample at stage A and the calibration sample at stage B simultaneously, and calibrates the energies for observing extremely small spectral shifts; for example, the 0.3 meV energy shift between the 100%-^{57}Fe-enriched $[Fe_4S_4Cl_4]^{=}$ and 10%-^{57}Fe and 90%-^{54}Fe labeled $[Fe_4S_4Cl_4]^{=}$ has been well resolved; (ii) a quick-switching energy calibration procedure, which reduces each calibration time from 3–4 h to about 30 min. Although the quick-switching calibration is not *in situ*, it is suitable for normal NRVS measurements.

Keywords: nuclear resonant vibrational spectroscopy; high-resolution monochromator; *in situ* energy calibration; quick-switching energy calibration; small energy shift; energy scale; energy position.

1. Introduction

Nuclear resonant vibrational spectroscopy (NRVS) scans an extremely monochromatic (~1 meV) X-ray beam through the nuclear resonance (*e.g.* ^{57}Fe at 14.4 keV) and measures the corresponding creation or annihilation of phonons (Seto *et al.*, 1995, 2009; Sturhahn *et al.*, 1995; Yoda *et al.*, 2001, 2012). It is a relatively new X-ray spectroscopy that became available because of the development of third-generation synchrotron sources, insertion devices and advanced X-ray optics. It has several distinguished advantages in comparison with traditional infrared (IR) and resonant Raman (RR) spectroscopies (Smith *et al.*, 2005) and has become an excellent pin-point tool in recent years for studying iron-specific inorganic and bioinorganic chemistry. For example, it revealed and resolved Fe-S/P/Cl and Fe-CO/CN/NO vibrational modes inside various chemical or enzymatic molecules (Smith *et al.*, 2005; Xiao *et al.*, 2005, 2006; Tinberg *et al.*, 2010; Do *et al.*, 2011; Kamali *et al.*, 2013).

The energy of the high-resolution monochromator (HRM) used for NRVS can be scanned (or altered involuntarily) by changing: (i) the relative scattering angles among the HRM crystals; and/or (ii) the temperature of one back-reflection crystal (Zhao & Sturhahn, 2012). The accuracy for the energy scale therefore relies on the high-precision measurements (and controls) on the angle, the temperature, as well as the thermal gradients for the HRM crystals. The error is usually about a few percent of the HRM energy. For higher accuracy, additional calibration is required (Zhao & Sturhahn, 2012). NRVS, especially on biological samples, has a very weak signal level and needs about 24–48 h (Kamali *et al.*, 2013) to obtain a quality spectrum for a dilute sample. During such a long period, the energy position/scale becomes a particular issue for obtaining good statistics for the targeted weak spectral peak(s), and should be frequently calibrated. In addition, a careful and scan-by-scan calibration is absolutely necessary for observing small shifts between different NRVS spectra.

A conventional NRVS calibration is performed by measuring a standard calibration sample (CS) in the main NRVS chamber. The procedure includes: (i) warming up the cryostat base to 140–200 K (Wang *et al.*, 2012); (ii) taking the existing NRVS sample out of the chamber (cryostat); (iii) loading in the CS; (iv) cooling down the CS (*e.g.* to 10 K; sensor reading); and (v) measuring the CS. In practice, the first

two NRVS spectra have slightly irreproducible peak positions, which could be due to the gradual transition of the real sample temperature (Wang *et al.*, 2012). The overall procedure usually takes about 3–4 h. This time-consuming nature makes a frequent energy calibration impractical.

Meanwhile, samples under X-ray irradiation could have stored energy inside the molecule. The 'radiation damage' may be 'frozen' under cryogenic temperatures (LT) (Garman & Nave, 2009). Taking the samples off the cryostat base means warming up the sample and increasing the chance of radiation damage, which should be avoided if possible. This makes it impossible to perform an energy calibration during one NRVS measurement, which could be as long as 48 h for a dilute sample [*e.g.* on NiFe hydrogenase (Kamali *et al.*, 2013)]. Thus, alternative calibration procedures without moving the NRVS sample out of the cryostat must be explored for biological NRVS measurements.

In a recent publication, Zhao & Sturhahn (2012) reported a successful procedure to calibrate HRM energy using the detailed-balance between the phonon annihilation and the phonon creation in an iron foil (or in any samples), with minor changes in the NRVS measurement set-up. This is a sample-independent method and does not require a specified standard sample. It also provides an accurate energy ruler (including the higher-order corrections) for an interested HRM. However, their procedure takes about 4 h (Zhao & Sturhahn, 2012), which still limits its application as a frequent energy checkup during regular NRVS measurements.

In this study, by manipulating the 14.4 keV beam through the main measurement chamber [Figs. 1(*a*) and 1(*b*)] without moving the main sample out of the cryostat, two alternative calibration procedures have been tested and developed: (i) an *in situ* calibration procedure, which measures the main NRVS sample and the calibration sample simultaneously; (ii) a quick-switching energy calibration procedure, which reduces each calibration time dramatically and makes a frequent energy calibration possible.

2. Experiment details

2.1. NRVS measurements at stage A

The NRVS beamline at SPring-8, BL09XU, has been described in detail elsewhere (Seto *et al.*, 2009; Yoda *et al.*, 2012) and is re-illustrated in Fig. 1(*a*). The synchrotron-radiation-produced X-rays were first converted into a beam with E = 14.4 keV and ΔE = 1 eV by a high-heat-load monochromator; it was then further converted into a beam with E = 14.4 keV and $\Delta E \simeq 1$ meV by a HRM. The photon flux at 14.4 keV was then $\sim 1.4 \times 10^9$ photons s^{-1} with a 0.8 meV energy bandwidth, or $\sim 2.5 \times 10^9$ photons s^{-1} with a 1.1 meV energy resolution. The beam size was about 0.6 mm (height) × 1 mm (width). The stage A is for NRVS measurements and the stage B is for energy calibration measurements. The measurement hutch for stage A and stage B is shown in Fig. 1(*b*).

At stage A, NRVS spectra were recorded using a standard experimental procedure on a standard set-up with a liquid-helium (LHe) flow cryostat (Smith *et al.*, 2005; Xiao *et al.*, 2005). The spectra were generally measured from −30 meV to 70–100 meV, depending on the sample. Delayed nuclear fluorescence and Fe $K\alpha$ fluorescence were recorded with a

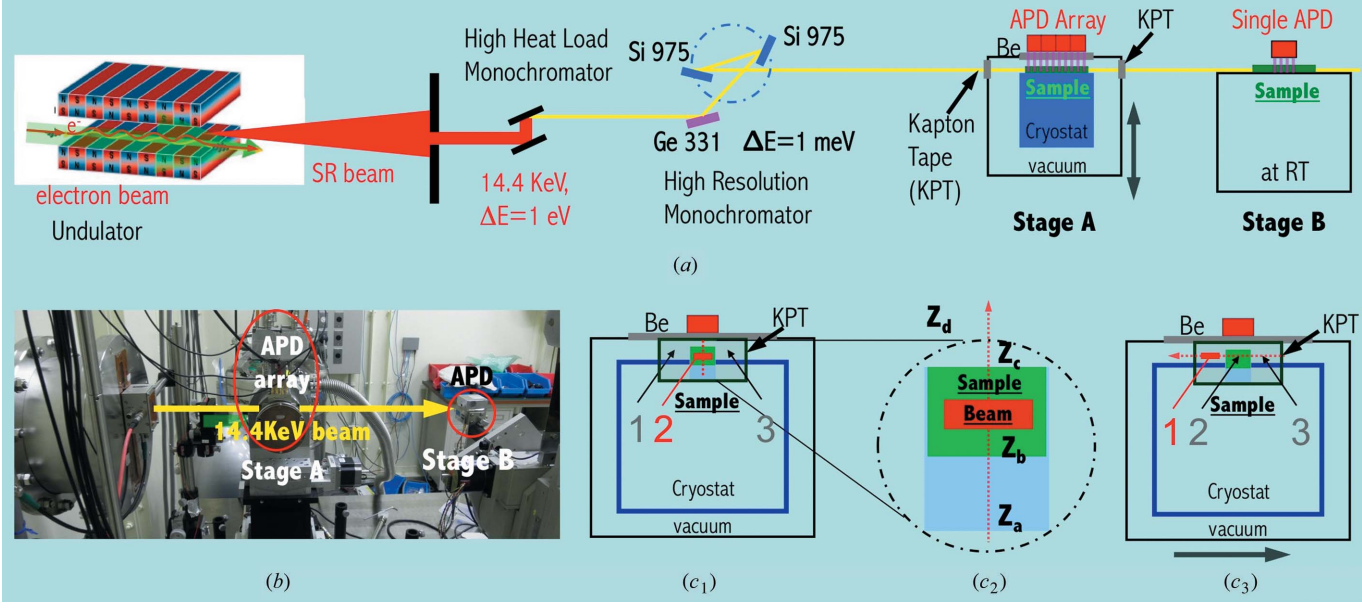

Figure 1
(*a*) Schematic illustration of SPring-8 BL09XU beamline with its main measurement chamber at cryogenic temperature at stage A and the calibration set-up at room temperature at stage B. (*b*) Photograph of the NRVS measurement hutch at BL09XU, showing the stages A and B. The thick yellow arrow indicates the E = 14.4 keV and $\Delta E \simeq 1$ meV X-ray beam. (*c*) Schematic and cross-section view (against the beam direction) of the main measurement chamber at stage A. The red bar represents the beam position relative to the NRVS sample for a Z scan (c_1, and c_2 with an expanded view) and an X scan (c_3).

2×2 avalanche photodiode (APD) detector array and processed with data-acquisition electronics. The maximum resonant peaks were different from sample to sample (*e.g.* 100–2000 counts s^{-1}). NRVS spectral analysis was performed using the *PHOENIX* software package (Sturhahn *et al.*, 1995), where the observed raw NRVS spectra were calibrated (to the nuclear resonant peak), normalized (to the I_0 variation), summed and converted to the ^{57}Fe partial vibrational density of states (PVDOS). Either NRVS or PVDOS in the following text actually means a PVDOS spectrum unless it is specified with raw NRVS.

2.2. Passing beam through stage A

At stage A, there is a ~1 mm space between the sample's top surface and the main chamber's beryllium window (Wang *et al.*, 2012), as illustrated in Figs. 1(c_1) and 1(c_2). Part of the 14.4 keV beam can pass through the sample at stage A and part of it can pass through the ~1 mm space to reach the sample at stage B. The simultaneous NRVS measurements on samples at A and B constitute an *in situ* calibration.

Figs. 2(*a*) and 2(*b*) exhibit the signal levels (counts s^{-1}) for Fe NRVS measured at B under several circumstances: (i) there is about a 2.7 mm space for the beam passage when an empty cryostat base is in the main chamber at stage A (black curve, between positions Z_a and Z_d); (ii) there is about a 1.8 mm space with an empty Lucite sample holder (blue, between Z_b and Z_d); (iii) the space is reduced to ~0.4 mm and the signal level drops to ~50% with a real $[Fe_4S_4Cl_4]^=$ sample at A (red, between Z_c and Z_d). These sizes are in general consistent with the real structural sizes. The positions Z_a, Z_b, Z_c and Z_d are the same as in Fig. 1(c_2). The green curve shows the NRVS signal of $[Fe_4S_4Cl_4]^=$ at A.

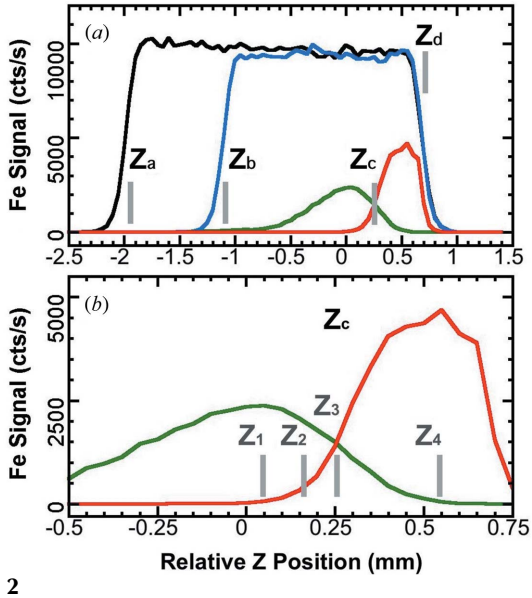

Figure 2
(*a*) Fe NRVS signal at B (black, blue and red) *versus* the relative beam positions (Z): the black curve is for an empty cryostat base; the blue is for an empty sample holder; the red is for a real sample ($[Fe_4S_4Cl_4]^=$) at A. Letters Z_a, Z_b, Z_c and Z_d indicate the cut-off at the cryostat base, sample holder's inner bottom, sample's top surface and vacuum chamber's top window, respectively. (*b*) Blow-up of (*a*). The bars Z_1, Z_2, Z_3 and Z_4 are several possible choices for an *in situ* calibration. The green line represents the $[Fe_4S_4Cl_4]^=$ NRVS signal at A.

There are also spaces on the left-hand and right-hand sides of the main sample at A, as illustrated in Fig. 1(c_3) (positions 1 or 3). These spaces can also be utilized to allow the X-ray beam pass. In our practice, the best result was obtained by moving the stage A to the right for X = 4 mm [Fig. 1(c_3), position 1]. Stage A's height (Z) and tilting angle (θ) also need minor optimization for a complete beam passage. The positions for the NRVS measurement (at A) and for the energy calibration (at B) can be switched back and forth [$(X_1, Z_1, \theta_1) \longleftrightarrow (X_2, Z_2, \theta_2)$] in 1 or 2 mins rather than in 1 h for a sample change process. Therefore the second procedure is called the quick-switching calibration procedure.

2.3. NRVS measurements at stage B

At approximately 1 m behind stage A, stage B was set up to use the beam passing through A [Figs. 1(*a*) and 1(*b*)] for energy calibration measurements. The NRVS measurement procedure at B is the same as at A, but with a single-element APD. Powder ^{57}Fe or ^{57}Fe-enriched Fe_2O_3 was used as the calibration samples for our new calibration measurements. The calibration measurements at B were performed at room temperature (RT).

2.4. Samples

Powder sample $[Et_4N][^{57}FeCl_4]$ ($[FeCl_4]^-$ for short) (Smith *et al.*, 2005) was synthesized at the University of Michigan and was used as the standard sample in a conventional energy calibration procedure at stage A (Smith *et al.*, 2005; Xiao *et al.*, 2005, 2006). Powders of ^{57}Fe or ^{57}Fe labeled Fe_2O_3 were purchased from Isoflex (San Francisco, CA, USA), and were used for our new calibration procedures at stage B. For associated experiments, $^{57}Fe(edt)(CO)_2(PMe_3)_2$ (Guo *et al.*, 2008) was synthesized at the University of Illinois at Urbana Champaign; $(NH_4)_2Mg^{57}Fe^{II}(CN)_6$ {or $[MgFe(CN)_6]^=$} (Chumakov & Rüffer, 1998) was measured at ESRF BL18 and cited here. All the above samples are ^{57}Fe labeled. Natural abundance $KGdFe^{II}(CN)_6$ and $KEuFe^{II}(CN)_6$ {or $[EuFe(CN)_6]^-$ and $[GdFe(CN)_6]^-$} (Shokouhimehr *et al.*, 2010; Huang *et al.*, 2010) were synthesized at Kent State University. The 100%-^{57}Fe and 10%-^{57}Fe/90%-^{54}Fe labeled $[Fe_4S_4Cl_4](Ph_4P)_2$ samples ($[Fe_4S_4Cl_4]^=$ and $[^XFe_4S_4Cl_4]^=$ for short in the following text) were prepared at the University of California at Davis.

Details for non-calibration samples measured at stage A are omitted.

3. Results and discussions

3.1. A conventional calibration

Omitting the higher-order corrections (Zhao & Sturhahn, 2012), the real energy position can be calculated with $E_{real} = (KE_{obs}+\Delta E)$, where E_{real} stands for the real energy, E_{obs} stands for the observed energy, ΔE is the energy position drift and K is the energy scale. The energy calibration thus includes:

(i) aligning the nuclear resonant peak to $E = 0$ to correct for ΔE; (ii) rescaling the energy axis to obtain the correct K value. Part (i) is in general obtained automatically during the PHOENIX analyses. At BL09XU, the scanning software also includes a procedure to automatically re-align the $E = 0$ position prior to each scan. For (ii), K is calculated by comparing the observed and the published $[FeCl_4]^-$ NRVS spectrum (Smith *et al.*, 2005). The published standard spectrum has the same peaks in its IR spectrum (Smith *et al.*, 2005). The above procedure is outlined figuratively in Fig. S1(*a*) and S1(*b*) in the supplementary information, while a series of $[FeCl_4]^-$ calibrated K values are also illustrated in Fig. S2.[1] The obtained K values appear to be between 0.938 and 0.976, a span of about 4%, which is not unexpected for a HRM (Zhao & Sturhahn, 2012).

As a conventional calibration takes time, the practical calibration interval was about 72 h. For more frequent energy calibrations, alternative procedures have to be developed.

3.2. An *in situ* calibration

There are two types of energy calibration procedures in general: (i) scan-by-scan calibrations and (ii) several calibrations during one beam time. An *in situ* calibration is a scan-by-scan calibration to track well the energy position/scale. As shown in Fig. 3(*a*), it seems impossible to distinguish the spectra with a 0.1% difference in their energy scale. On the other hand, it is clear to distinguish the spectra with a 0.3% difference (Fig. 3*b*). Although it is not rigid, 0.2–0.3% could be used as a practical guide for a clear identification of a spectral shift. The expanded spectra in Figs. 3(*c*) and 3(*d*) provide a better illustration of this practical limit.

The first task for our *in situ* calibration is to establish the correlation between the new (Fe or Fe_2O_3) and the old ($[FeCl_4]^-$) standard spectra. The results are shown in Figs. 4(*a*) and 4(*b*). A sample selected for the calibrations at stage B needs to have several properties: (i) it must be chemically stable in air at RT; (ii) its NRVS or PVDOS spectrum at RT needs to have sharp feature(s); and (iii) it must have a high signal level (counts s^{-1}). Powder Fe has a prominent peak at 35.6 meV in both raw NRVS and converted PVDOS. Powder Fe_2O_3 has multiple peaks, including ones at 35.7, 41.0, 46.9, 50.1 meV, in its PVDOS. Under current experimental conditions, Fe has about 10000 counts s^{-1} while Fe_2O_3 has about 15000 counts s^{-1}. The higher counts s^{-1} for Fe_2O_3 is probably due to the wider absorption width (the larger magnetic splitting in the case of thick samples). Therefore both samples are good for the new calibration procedures. At RT, $[FeCl_4]^-$ does not have a sharp peak, and it has only 800 counts s^{-1}.

The second task is to observe extremely small energy shifts. Owing to a careful *in situ* calibration, such as the one shown in Fig. 5(*a*), a small isotopic shift of 47.5 → 47.8 meV (0.3 meV, or 0.63%) was observed and resolved for $[Fe_4S_4Cl_4]^=$ → $[^XFe_4S_4Cl_4]^=$ (Fig. 5*b*). The expanded NRVS spectra are presented in Fig. 5(*c*) to better illustrate this 0.3 meV shift. As discussed in detail in the supplementary information, a $[^XFe_4S_4Cl_4]^=$ complex has a combination of ^{57}Fe and ^{54}Fe sites, and a mixed NRVS signal from $[^{57}Fe_2{}^{54}Fe_2S_4Cl_4]^=$ (25%) and

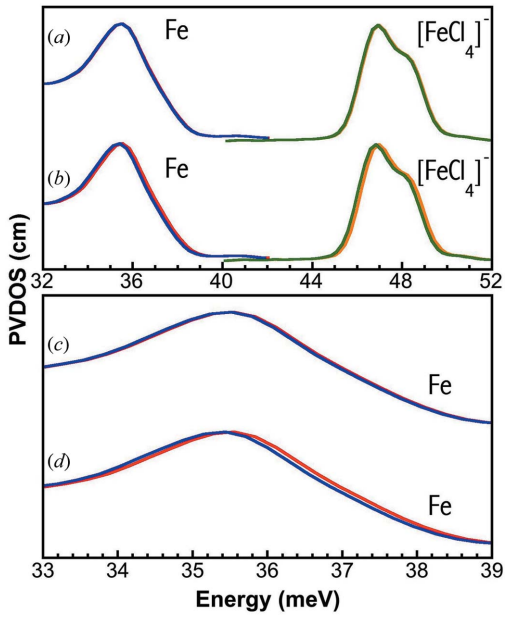

Figure 3
Calibrated NRVS of Fe (red) and $[FeCl_4]^-$ (orange) *versus* their copies with 99.9% (*a*) and 99.7% (*b*) scaled energy axis (blue and green). There is no observable difference between the original and scaled NRVS in (*a*), while there is a clear difference between the two spectra in (*b*). (*c*) and (*d*) are the expanded versions of (*a*) and (*b*), respectively.

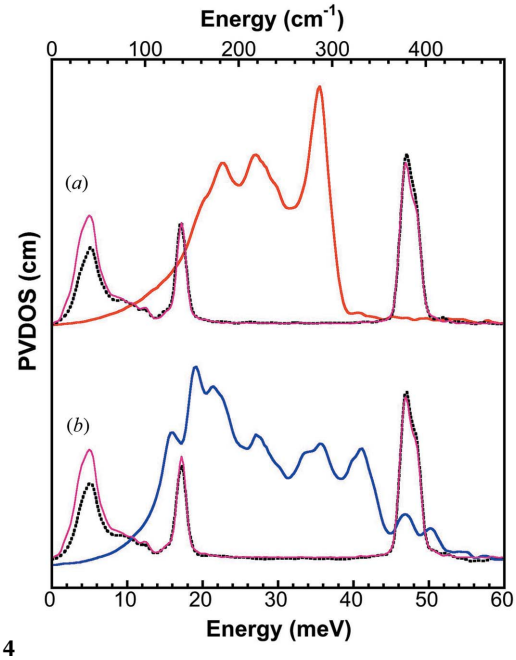

Figure 4
PVDOS measured at stages A and B simultaneously: (*a*) observed $[FeCl_4]^-$ at A (×0.5, dashed black) *versus* observed Fe at B (solid red); (*b*) observed $[FeCl_4]^-$ at A (×0.5, dashed black) *versus* observed Fe_2O_3 at B (×2, solid blue). The solid purple curve is the standard PVDOS for $[FeCl_4]^-$ (Smith *et al.*, 2005).

[1] Supplementary data for this paper are available from the IUCr electronic archives (Reference: MO5055). Services for accessing these data are described at the back of the journal.

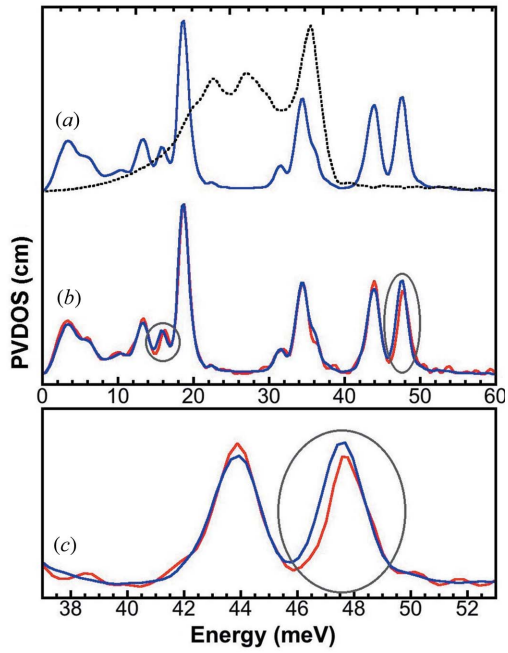

Figure 5
(*a*) PVDOS of $[Fe_4S_4Cl_4]^=$ at A (solid blue) *versus* Fe powder at B (dashed black). (*b*) Fe calibrated PVDOS of $[Fe_4S_4Cl_4]^=$ (blue) *versus* $[^XFe_4S_4Cl_4]^=$ (red). (*c*) Expanded spectra of (*b*).

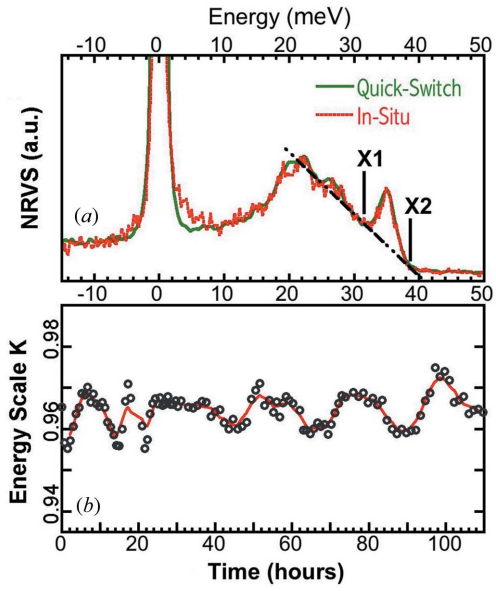

Figure 6
(*a*) Raw ^{57}Fe powder NRVS measured with a quick-switching procedure (solid green) and a semi *in situ* procedure (using five-scan-averaged spectra, dashed red). *X*1 and *X*2 signify the integration range for the Fe 35.6 meV peak (32–39 meV). (*b*) ^{57}Fe powder monitored semi *in situ* energy scales *K* *versus* time. The open symbols are analyzed from single Fe scans and the red solid line is from the five-scan-averaged spectra.

$[^{57}Fe^{54}Fe_3S_4Cl_4]^=$ (75%) species. A simple Fe—S stretching estimation indicates a 0.33 meV spectral shift between $[Fe_4S_4Cl_4]^=$ and $[^XFe_4S_4Cl_4]^=$, which is consistent with the observed 0.3 meV.

Small isotopic shifts are often useful for identifying metal-involved vibration(s). For example, (i) in a RR experiment (Mascarenhas *et al.*, 1989), the 1.8 cm^{-1} down-shift at 148.6 cm^{-1} by substituting ^{65}Cu for ^{64}Cu concluded that the peak is the Cu-involved vibration(s) in $YBa_2Cu_2O_{7-X}$, while the invariable 112.5 cm^{-1} peak does not involve Cu at all; (ii) with IR (Zhou *et al.*, 2013), the 2 to 3 cm^{-1} energy difference between ^{100}Mo/^{92}Mo labeled Mo homocitrate complexes identified the Mo═O and Mo—O bands inside the complex; and (iii) in NRVS, the small ^{57}Fe/^{54}Fe isotopic shift between $[Fe_4S_4Cl_4]^=$ and $[^XFe_4S_4Cl_4]^=$ can help pin-point the Fe—S vibrations as well (Mitra *et al.*, 2011).

As mentioned in §2.2, the measurements at A and at B cannot be optimized simultaneously. More signal for a NRVS measurement at A means less signal for the energy calibration at B and *vice versa*. Thus a balanced compromise has to be reached between the two samples. In measuring $[Fe_4S_4Cl_4]^=$, which has a maximum signal level of 2350 counts s^{-1}, the signal for A ($[Fe_4S_4Cl_4]^=$, green) and for B (Fe, red) are well balanced at position Z_3 if the energy calibration is the focus, as illustrated in Fig. 2(*b*). At this position, both samples have ∼1400 counts s^{-1}, corresponding to 62% of the $[Fe_4S_4Cl_4]^=$ peak value and 31% of the Fe's maximum (the maximum under the circumstance of an *in situ* calibration). In measuring $[^XFe_4S_4Cl_4]^=$ (maximum NRVS signal = 255 counts s^{-1}), the sample at A has 155 counts s^{-1} while Fe powder at B still has 1400 counts s^{-1}.

3.3. A semi *in situ* calibration

When the NRVS measurement rather than energy calibration is the focus, one no longer has the luxury to sacrifice 38% of the NRVS signal. In these cases, Z_2 (Fig. 2*b*) becomes an alternative position, which sacrifices ∼15% of the NRVS signal and has a much weaker (350 counts s^{-1} or ∼7.5% of its maximum level) and noisier calibration signal. Although single scans may not be good for tracking the energy scale scan-by-scan, few-scan-averaged spectra are still good for energy calibration. For example, as shown in Fig. 6(*a*), (i) a five-scan-averaged semi *in situ* calibration spectrum (dashed red) overlaps well with the one observed with a quick-switching calibration (solid green); and (ii) the sharp peak at 35.6 meV is still clear. To further improve statistics, the centroid, instead of the peak position, were used in the calibration procedure. We call this procedure semi *in situ* calibration.

Semi *in situ* calibrated *K* values *versus* the time for one beam time are illustrated in Fig. 6(*b*). The single-scan-calculated *K* values (black circles) look scattered, and probably do not reflect the real *K* values from scan to scan. On the other hand, the *K* values obtained from the five-scan-averaged spectra (red line) seem reasonably stable. The single-scan-derived data vary between 0.955 and 0.975 (2.0%) for a period of about 110 h while the five-scan-probed values vary from 0.957 to 0.973 (1.6%). The maximum difference between the neighboring *K* values is 0.4%.

The *K* variation trend seems to be more or less following a 24 h circle. This is consistent with the period of the environmental temperature circle.

3.4. A quick-switching calibration

As mentioned above, an *in situ* calibration either sacrifices the signal level in the NRVS measurement at A (§3.2) or results in a poor signal level for the energy calibration at B (§3.3). Therefore, a quick-switching calibration procedure was developed to swap between the two events without changing NRVS samples. As the calibration sample at B is always at one temperature (RT), the systematic irreproducible peak positions for the first two scans (with a conventional calibration) were never observed. Consequently, a single scan is good enough for one energy calibration. With this procedure, NRVS measurements and energy calibrations can use the full beam flux alternatively.

Although it is not an *in situ* calibration method, the less required calibration scans and the fast switching time reduce each energy calibration time from 3–4 h to about 30 min and thus the calibration interval from 72 h to as short as 6 h. A series of Fe_2O_3 calibrated K values during one particular beam time are illustrated in Fig. 7(*a*) (blue circles). The overall variation is between 0.951 and 0.965, about 1.4% difference. Another series of Fe calibrated K values for a separate beam time are shown in Fig. 7(*b*) (0.948–0.958 or 0.8%). The maximum calibration-to-calibration difference is 0.8% (only one case) and the average difference is 0.4% using all our quick-switching calibrated K values.

A 6 h interval is recommended because: (i) we noticed that all the calibrations with a 6 h interval have a maximum calibration-to-calibration difference of 0.6% (instead of 0.8%); (ii) it will cover the possible minima and maxima in the K values, assuming a 24 h thermal circle. When a 6 h calibration is not possible, an alternating 12–18–12–18 h interval is recommended instead. Incidents, such as entering the monochromator hutch or having a long time beam disruption, could change a HMR crystal's temperature by over 0.1° and produce a few percent change in the HRM's energy scale (K). This effect may need hours to recover. During the recovery period, more frequent calibrations are recommended to monitor the real HRM energy.

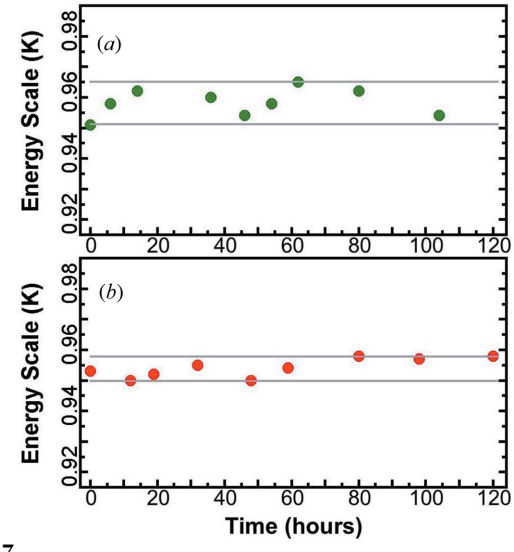

Figure 7
Energy scales (K values) obtained with Fe_2O_3 PVDOS (*a*) and with Fe PVDOS (*b*) using a quick-switching calibration procedure for two different beamtimes.

Table 1
Sizes of some common isotopic shifts in iron-related Fe—X stretching modes.

^{57}Fe—^{N}X stretches	^{57}Fe—C	^{57}Fe—N	^{57}Fe—O	^{57}Fe—S
Isotopes (^{N}X)	^{12}C/^{13}C	^{14}N/^{15}N	^{16}O/^{18}O	^{32}S/^{36}S
ΔE (estimated)	3.2%	2.7%	3.9%	3.6%
ΔE (observed)	3.8%	2.2%	5.7%	3.8%

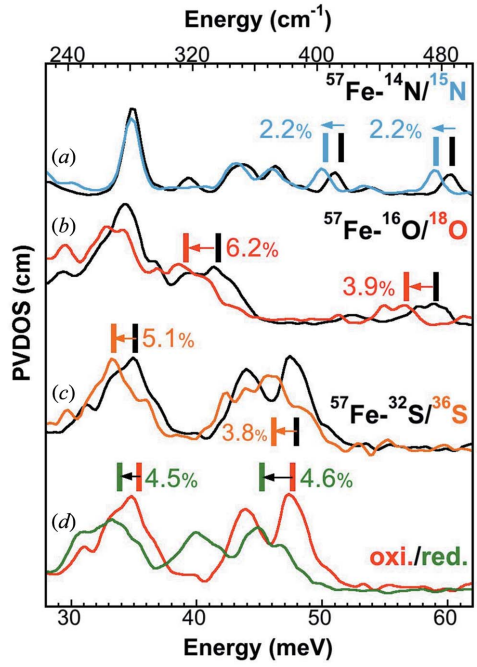

Figure 8
Various spectral shifts in typical NRVS: (*a*) the ^{14}N/^{15}N shifts in $(Et_4N)[Fe_4S_3(NO)_7]$ (Tonzetich *et al.*, 2010); (*b*) the ^{16}O/^{18}O shifts in $[Fe(\mu\text{-O})(N\text{-EtHPTB})(PhCO)]^+$ (Do *et al.*, 2011); (*c*) the ^{32}S/^{36}S shifts in *P. furiosis* ferredoxin (containing a Fe_4S_4 cluster) (Mitra *et al.*, 2011); (*d*) the redox shift for *P. furiosis* ferredoxin (Mitra *et al.*, 2011).

Is a 0.4–0.8% calibration precision good for an ordinary NRVS measurement? Let us see a few examples. Assuming a standalone iron–ligand stretch, Table 1 summarizes some common isotopic shifts, such as ^{57}Fe—^{12}C/^{13}C (Kamali *et al.*, 2013), ^{14}N/^{15}N (Tonzetich *et al.*, 2010), ^{16}O/^{18}O (Do *et al.*, 2011) and ^{32}S/^{36}S (Mitra *et al.*, 2011). Figs. 8(*a*)–8(*c*) also illustrate several observed examples of isotope shifts between ^{14}N/^{15}N, ^{16}O/^{18}O and ^{32}S/^{36}S. These theoretical and observed isotope shifts are of the order of 3–4% of the vibrational peak positions. Fig. 8(*d*) illustrates an example of a redox shift in Fe—S, which is ∼4.6%. Therefore a quick-switching calibration is quite suitable for observing the above spectral shifts.

3.5. Future perspectives

A higher-energy calibration peak will lead to a lower calibration error bar. In addition, sectional scans are often useful to resolve critical but weak features, *e.g.* the Fe—CO/CN in a NiFe hydrogenase enzyme (Kamali *et al.*, 2013). To calibrate

sectional scans *in situ*, a calibration sample with a prominent peak in the same energy section (*e.g.* 60–80 meV) becomes necessary. Complex $[MgFe(CN)_6]^{=}$ has a sharp peak at ~75 meV (or 600 cm^{-1}) (Fig. 9*a*) and can be used to calibrate high-energy sectional scans.

Many similar complexes also exist. For example, potential medical MRI or cellular imaging agents $[GdFe(CN)_6]^{-}$ and $[EuFe(CN)_6]^{-}$ (Shokouhimehr *et al.*, 2010; Huang *et al.*, 2010) also have the Fe—CN peak roughly around 75 meV (Fig. 9*b*). The small peak drifts in these spectra without the elastic peak, in turn, illustrate the need for a standard sample with feature(s) in the same region to calibrate the energy axis (Fig. 9*b*).

A LT environment will also extend our choices for the calibration samples because many complexes are not stable at RT, but are very stable at LT. Fig. 9(*c*) illustrates the PVDOS for a model complex $Fe(edt)(CO)_2(PMe_3)_2$. The blue curve shows the initial spectrum measured in 2006 (Guo *et al.*, 2008) [sensor reading T = 10 K, real T = 100 K (Wang *et al.*, 2012)] while the red curve shows the spectrum measured in 2012 (sensor reading T = 120 K, real T = 140 K). The comparison shows that $Fe(edt)(CO)_2(PMe_3)_2$ is stable after six years stored in LN_2. This sample should be a good sample to calibrate the Fe—CO region if a LT chamber is available at B.

As calibration precision also depends on the signal level, it will be gratifying to see a further increase in the calibration signal at A without sacrificing more NRVS signal at A. Under the current experimental conditions, use of a multiple-element APD array is an immediate option; a LT environment, using a LHe cryostat (Xiao *et al.*, 2005), a LN_2 cryostat (77 K) (Dong *et al.*, 2013), or a thermoelectric cooling device (120 K) (Monroe, 2013), should also be useful to make spectral peaks sharper and background cleaner. In addition, more beam flux will be available in the future due to the continuous development in synchrotron radiation sources, insertion devices and beamline optics.

4. Summary

Two alternative energy calibration procedures have been successfully established. Neither of these requires removing NRVS samples out of the cryostat. An *in situ* calibration procedure tracks the energies scan-by-scan and is best for observing an extremely small spectral shift, such as the 0.3 meV difference between $[Fe_4S_4Cl_4]^{=}$ and $[^{X}Fe_4S_4Cl_4]^{=}$. A quick-switching calibration reduces the calibration time and calibration interval dramatically, and is suitable for observing general isotopic or redox shift, which is of the order of a few percent of the vibrational peak energy.

While Fe and Fe_2O_3 are good for calibrating regular vibrational modes (*e.g.* Fe—S at 14–54 meV), several $[XFe(CN)_6]^{-}$ (X = metal) complexes are found useful for calibrating high-energy features (*e.g.* Fe—CO at ~70 meV).

This work was funded by NIH grants GM-65440, EB-001962, and the DOE Office of Biological and Environmental Research (all to Professor Stephen P. Cramer at UC Davis).

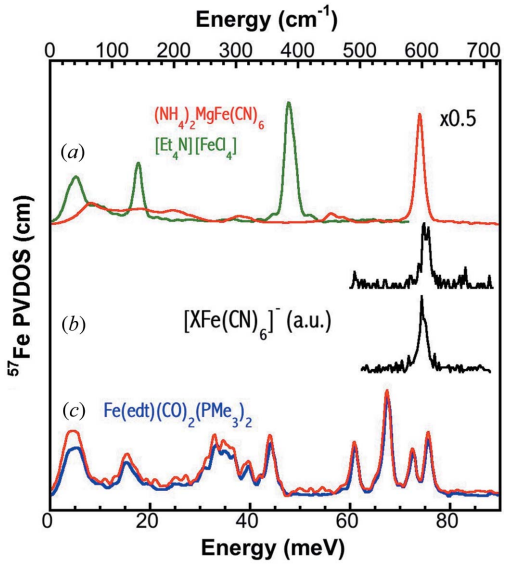

Figure 9
(*a*) PVDOS of $[MgFe(CN)_6]^{=}$ (red) at RT *versus* $[FeCl_4]^{-}$ at LT (green); (*b*) raw NRVS (a.u.) for non-enriched $[XFe(CN)_6]^{-}$ (X = Gd or Eu) at RT; (*c*) PVDOS of $Fe(edt)(CO)_2(PMe_3)_2$ six years saved under LN_2 (red, at 140 K) *versus* the fresh sample (blue, at 100 K).

The work at Kent State University was supported by NIH-NCI (1R21CA143408-01A1, to SDH). NRVS spectra were measured at SPring-8 BL09XU with the approval of JASRI (Proposal No. 2011A/B0032 and 2012A/B0032). We also thank Professor Cramer (at UC Davis) for the overall support, Dr Ilya Sergeev/Dr Aleksandr Chumakov (at ESRF/ID18) for assistance in obtaining the $[MgFe(CN)_6]^{=}$ NRVS, and Dr Jiyong Zhao (at APS 03ID) for discussion on HRM calibrations.

References

Chumakov, A. & Rüffer, R. (1998). *Hyperfine Interact.* **113**, 59–79.
Do, L., Wang, H., Tinberg, C. E., Dowty, E., Yoda, Y., Cramer, S. P. & Lippard, S. J. (2011). *Chem. Commun.* **47**, 10945.
Dong, W., He, P., Wang, J., Zhou, Z. & Wang, H. (2013). *Infrared Phys. Technol.* **56**, 51–56.
Garman, E. F. & Nave, C. (2009). *J. Synchrotron Rad.* **16**, 129–132.
Guo, Y., Wang, H., Xiao, Y., Vogt, S., Thauer, R. K., Shima, S., Volkers, P. I., Rauchfuss, T. B., Pelmenschikov, V., Case, D. A., Alp, E. E., Sturhahn, W., Yoda, Y. & Cramer, S. P. (2008). *Inorg. Chem.* **47**, 3969–3977.
Huang, S. D., Li, Y. & Shokouhimehr, M. (2010). US 2010/0215587A1.
Kamali, S., Wang, H., Mitra, D., Ogata, H., Lubitz, W., Manor, B. C., Rauchfuss, T. B., Byrne, D., Bonnefoy, V., Jenney, F. E., Adams, M. W. W., Yoda, Y., Alp, E., Zhao, J. & Cramer, S. P. (2013). *Angew. Chem. Int. Ed.* **52**, 724–728.
Mascarenhas, A., Katayama-Yoshida, H., Pankove, J. & Deb, S. (1989). *Phys. Rev. B*, **39**, 4699–4700.
Mitra, D., Pelmenschikov, V., Guo, Y., Case, D. A., Wang, H., Dong, W., Tan, M. L., Ichiye, T., Jenney, F. E., Adams, M. W., Yoda, Y., Zhao, J. & Cramer, S. P. (2011). *Biochemistry*, **50**, 5220–5235.
Monroe, D. (2013). *Physics*, **6**, 63.
Seto, M., Masuda, R., Higashitaniguchi, S., Kitao, S., Kobayashi, Y., Inaba, C., Mitsui, T. & Yoda, Y. (2009). *Phys. Rev. Lett.* **102**, 217602.

Seto, M., Yoda, Y., Kikuta, S., Zhang, X. W. & Ando, M. (1995). *Phys. Rev. Lett.* **74**, 3828–3831.
Shokouhimehr, M., Soehnlen, E. S., Hao, J., Griswold, M., Flask, C., Fan, X., Basilion, J. P., Basu, S. & Huang, S. D. (2010). *J. Mater. Chem.* **20**, 5251.
Smith, M. C., Xiao, Y., Wang, H., George, S. J., Coucouvanis, D., Koutmos, M., Sturhahn, W., Alp, E. E., Zhao, J. & Cramer, S. P. (2005). *Inorg. Chem.* **44**, 5562–5570.
Sturhahn, W., Toellner, T. S., Alp, E. E., Zhang, X., Ando, M., Yoda, Y., Kikuta, S., Seto, M., Kimball, C. W. & Dabrowski, B. (1995). *Phys. Rev. Lett.* **74**, 3832–3835.
Tinberg, C. E., Tonzetich, Z. J., Wang, H., Do, L. H., Yoda, Y., Cramer, S. P. & Lippard, S. J. (2010). *J. Am. Chem. Soc.* **132**, 18168–18176.
Tonzetich, Z. J., Wang, H., Mitra, D., Tinberg, C. E., Do, L. H., Jenney, F. E., Adams, M. W., Cramer, S. P. & Lippard, S. J. (2010). *J. Am. Chem. Soc.* **132**, 6914–6916.
Wang, H., Yoda, Y., Kamali, S., Zhou, Z.-H. & Cramer, S. P. (2012). *J. Synchrotron Rad.* **19**, 257–263.
Xiao, Y., Fisher, K., Smith, M. C., Newton, W. E., Case, D. A., George, S. J., Wang, H., Sturhahn, W., Alp, E. E., Zhao, J., Yoda, Y. & Cramer, S. P. (2006). *J. Am. Chem. Soc.* **128**, 7608–7612.
Xiao, Y., Wang, H., George, S. J., Smith, M. C., Adams, M. W., Jenney, F. E., Sturhahn, W., Alp, E. E., Zhao, J., Yoda, Y., Dey, A., Solomon, E. I. & Cramer, S. P. (2005). *J. Am. Chem. Soc.* **127**, 14596–14606.
Yoda, Y., Imai, Y., Kobayashi, H., Goto, S., Takeshita, K. & Seto, M. (2012). *Hyperfine. Interact.* **206**, 83–86.
Yoda, Y., Yabashi, M., Izumi, K., Zhang, X. W., Kishimoto, S., Kitao, S., Seto, M., Mitsui, T., Harami, T., Imai, Y. & Kikuta, S. (2001). *Nucl. Instrum. Methods Phys. Res. A*, **467**, 715–718.
Zhao, J. Y. & Sturhahn, W. (2012). *J. Synchrotron Rad.* **19**, 602–608.
Zhou, Z. H., Wang, H., Yu, P., Olmstead, M. M. & Cramer, S. P. (2013). *J. Inorg. Biochem.* **118**, 100–106.